Ligand Functionality as a Versatile Tool to Control the Assembly Behavior of Preformed Titania Nanocrystals

Julien Polleux,[a] Nicola Pinna,[a] Markus Antonietti,[a] Christian Hess,[b] Ute Wild,[b] Robert Schlögl,[b] and Markus Niederberger*[a]

Abstract: Nanoparticle powders composed of surface-functionalized anatase crystals with diameters of about 3 nm self-organize into different structures upon redispersion in water. The assembly is directed by a small amount of a low-molecular-weight functional ligand (the "assembler") adsorbed on the surface of the nanoparticles. The ligand functionality determines the anisotropy of the resulting structures. Multidentate ligands, such as trizma ($(HOCH_2)_3CNH_2$) and serinol ($(HOCH_2)_2CNH_2$), with a chargeable terminal group preferentially induce the formation of anisotropic nanostructures several hundreds of nanometers in total length, whereas all the other investigated ligands (ethanolamine $H_2N(CH_2)_2OH$, glycine hydroxamate $H_2NCH_2CONHOH$, dopamine $(OH)_2C_6H_3(CH_2)_2NH_3Cl$, tris $(HOCH_2)_3CCH_3$) mainly lead to uncontrolled agglomeration. Experimental data suggests that the anisotropic assembly is a consequence of the water-promoted desorption of the organic ligands from the {001} faces of the crystalline building blocks together with the dissociative adsorption of water on these crystal faces. Both processes induce the preferred attachment of the titania nanoparticles along the [001] direction. The use of polydentate and charged ligands to functionalize the surface of nanoparticles thus provides a versatile tool to control their arrangement on the nanoscale.

Keywords: anatase · nanoparticle assembly · nanostructures · nonaqueous synthesis · surface chemistry

Introduction

In addition to the synthesis of nanoparticles with controlled particle size, shape, and crystal structure, the main focus of nanochemistry shifts more and more towards the use of these nanoparticles as building blocks for the fabrication of one-, two-, and three-dimensional superstructures.[1–4] The continuing trend towards miniaturization, combined with an increase in performance and multifunctionality, is a major driving force for the exploration of such novel "bottom-up" approaches. Key requirements of a new nanofabrication technique are the ability to produce components with nanometer precision and the ability to control their assembly into functional devices.[5] In the last few years, many different methodologies of nanoparticle synthesis have been reported, covering a wide range of compositions, morphologies, and structures. Anisotropic structures, which are particularly promising as modules for nanodevices,[6] have been obtained in the form of nanowires,[7,8] nanotubes,[6,9] or nanobelts[10] mainly by the so-called vapor–liquid–solid growth,[11] thermal evaporation,[12] or template-directed synthesis approaches. In the last case, diverse molecular surfactants are used to control the anisotropic particle growth.[13–16] Another promising, but yet much less investigated, approach for the preparation of one-dimensional (1D) nanostructures is based on the spontaneous self-assembly of preformed, individual, and crystalline nanoparticles. One of the few examples is the spontaneous organization of nanoparticles into luminescent CdTe nanowires.[17,18] The key step in this process was the controlled removal of the protective shell provided by the organic stabilizer, thioglycolic acid, from the nanoparticles. After the formation of a pearl-necklace aggregate, the linear assemblies recrystallized into wires. Another example is based on the oriented attachment of preformed quasi-spherical ZnO nanoparticles leading to the formation of single-crystal nanorods.[19] Also in or-

[a] J. Polleux, Dr. N. Pinna, Prof. Dr. M. Antonietti, Dr. M. Niederberger
Max-Planck-Institute of Colloids and Interfaces
Colloid Chemistry, Research Campus Golm
14424 Potsdam (Germany)
Fax: (+49) 331-567-9502
E-mail: markus.niederberger@mpikg.mpg.de

[b] Dr. C. Hess, U. Wild, Prof. Dr. R. Schlögl
Fritz–Haber-Institute of the Max-Planck-Society
Department of Inorganic Chemistry, Faradayweg 4–6
14195 Berlin (Germany)

 DOI: 10.1002/chem.200401050

ganic chemistry, the crystallization of dyes[20] or DL-alanine[21] by directed aggregation of colloidal intermediates was reported, providing a model case for this nonclassical mesoscopic crystallization process.

The synthesis of titanium oxide (TiO_2) nanomaterials is a particularly attractive objective with respect to applications in photocatalysis,[22] photovoltaics,[23,24] photochemical water splitting,[25] and sensing.[26] The large surface-to-volume ratio of anisotropic nanostructures results in a favorable combination of high specific surface areas with improved conduction paths, having significant implications for solar energy conversion and photocatalysis.[27] For the synthesis of anisotropic TiO_2, two methodologies have mainly been applied, namely, surfactant-assisted methods and oriented attachment of TiO_2 nanocrystals. In the former case, the lateral expansion of the crystal lattice has to be suppressed to achieve anisotropic crystal growth, usually by adding a large excess of surfactant, such as oleic acid.[28] Oleic acid plays two roles, namely, as stabilizing solvent and as chemical modifier to control the hydrolysis rate of the titanium alkoxide precursor. Better fine-tuning of the growth rate of the different crystal faces, and thus, control over the shape evolution of the anatase nanocrystals, has been obtained by the use of mixtures of surfactants, which selectively bind to different crystal faces and eliminate high-energy facets.[29] This method relies on the fact that the crystal growth is determined by the different surface energies of the crystal faces, and the surface energy is either enhanced or reduced by surfactant adhesion, using lauric acid (LA) as the surface-selective surfactant and trioctylphosphine oxide (TOPO) as the nonselective surfactant. However, anisotropic crystal growth resulting in the formation of anatase nanorods was only obtained at a Ti-to-LA ratio of less than one, which means that the selective surfactant was always present in large excess relative to the amount of Ti atoms on the {001} faces.

Oriented attachment involves spontaneous self-organization of adjacent particles, so that they share a common crystallographic orientation, followed by joining of these particles at a planar interface.[30–32] Penn et al. reported the formation of anisotropic aggregates during hydrothermal treatment of TiO_2 nanocrystals under acidic conditions by oriented attachment.[33] However, hydrothermally induced assembly processes are difficult to control and a better approach to controlled assembly behavior might involve the adsorption of polydentate, low-molecular-weight ligands onto the surface of the nanoparticles in a crystallographically selective manner, leading to differentially functionalized crystal faces. Based on these ideas, we recently reported a simple strategy to synthesize and assemble functionalized titania nanoparticles into highly anisotropic nanostructures of several hundred nanometers in total length.[34] The formation of these pearl-necklace agglomerates was a direct consequence of the two-step procedure, which included the nonaqueous in situ functionalization process for the preparation of the titania nanoparticles functionalized with an aminotrialcohol, and the subsequent assembly of the particles into anisotropic nanostructures in water by means of oriented attachment. It is an outstanding feature of this process that a particularly small amount of the directing ligand (the "assembler") not only allows the modification of the surface, and thus, the control of the assembly, but also influences the size and shape of the nanoparticles during the synthesis. The observation that the agglomeration of the particles occurs mainly along the [001] direction, albeit with some misorientations, points to the fact that the ligands are bound or removed in a crystallographically selective manner, resulting in the stabilization of all exposed crystal faces except the {001} faces.

Recent work has also shown that nonaqueous synthesis methods provide a generally applicable tool to obtain surface-functionalized nanoparticles.[35,36] For example, synthesis protocols based on the reaction of metal oxide precursors, such as metal halides or metal alkoxides, with benzyl alcohol allow the preparation of a large variety of binary[37,38] and ternary metal oxide nanoparticles,[39,40] with excellent control over particle size,[41] shape,[42] crystallinity, and surface functionalization.[43] Nanoparticles, for example, of SnO_2 and In_2O_3, obtained by the "benzyl alcohol route" have already shown their high potential for applications in gas sensing.[44]

In the present work, fabrication of well-defined nanostructures, consisting of nanosized building blocks of functionalized anatase, was achieved using the "benzyl alcohol

Abstract in French: *Selon les fonctions chimiques présentes en surface, les nanocristaux d'anatase obtenus sous forme de nanopoudres ont la propriété de s'auto-organiser en différentes nanostructures après redispersion dans l'eau. L'assemblage est dirigé par la présence de molécules organiques de faible masse molaire, adsorbées à la surface des nanoparticules, dont les fonctions chimiques déterminent si l'assemblage s'effectue de façon anisotropique ou non spécifique. Comme le trizma $(HOCH_2)_3CNH_2$ et le sérinol $(HOCH_2)_2CHNH_2$, les polyalcools aminés présentant des groupes terminaux chargés induisent préférentiellement la formation de nanostructures anisotropiques de plusieurs centaines de nanomètres de long, tandis que les autres types de ligands étudiés (éthanolamine $H_2N(CH_2)_2OH$, hydroxamate de glycine $H_2NCH_2CONHOH$, dopamine $(OH)_2C_6H_3(CH_2)_2NH_3Cl$, tris $(HOCH_2)_3CCH_3$) n'aboutissent qu'à un assemblage aléatoire des nanocristaux. Les données expérimentales supposent que l'assemblage anisotropique est la conséquence d'une désorption spécifique promue par l'eau des ligands liés aux plans {001} composant la surface des building blocks et simultanément, d'une adsorption dissociative des molécules d'eau sur ces plans cristallins. Ces deux effets privilégient l'attachement orienté des nanoparticules d'oxide de titane selon la direction [001]. L'utilisation de ligands chargés et polydentés afin de fonctionnaliser la surface de nanoparticules s'avère être un outil complet pour contrôler leurs propriétés de solubilité et d'organisation à l'échelle nanométrique permettant la fabrication de nanostructures par une approche bottom-up.*

route" for the preparation of anatase nanopowders, followed by redispersion and assembly in water. To elucidate the role of the functional groups of the "assembler" during the formation of the nanostructures, we systematically investigated the assembly behavior of the titania nanoparticles and its dependence on the ligand types attached to the surface of the particles. The ligands consist of an anchoring part binding to the titania surface and a terminal group pointing away from the particle core. We studied three families of ligands, with the main focus directed towards the comparison of unidentate with multidentate ligands and also the comparison of charged with uncharged terminal groups. In contrast to the surfactant-assisted methods, the assembly process, using preformed nanoparticles and a particularly low concentration of low-molecular-weight "assembler" molecules, bears the advantage of keeping the amount of organic impurities very low.

Results and Discussion

Different "assemblers" and their influence on the agglomeration behavior of preformed titania nanoparticles were investigated in detail. The molar ratios were kept constant as follows (BA = benzyl alcohol): Ti/BA = 1/20, Ti/"assembler" = 12 and BA/"assembler" = 240.

All of the differently functionalized TiO_2 nanoparticles were analyzed by X-ray diffraction (XRD). The corresponding powder diffraction patterns are shown in Figure 1. The diffraction peaks can be assigned to the anatase phase. However, a small shoulder frequently occurring on the higher angle side of the anatase (101) peak points to the presence of small amounts of brookite.[45] All particle sizes discussed in the following paragraphs were calculated from the (101) reflection of anatase by using Scherrer's equation. Although particle-size determination by peak broadening is just a rough estimation, the results coincide well with the transmission electron microscopy (TEM) data. A closer look at the XRD patterns shows some peculiar features, mainly related to the relative intensities of the (004) and (200) reflections, representing the *c* and *a* axes, respectively. In the case of the reference and serinol ($(HOCH_2)_2CNH_2$) samples, the (004) reflection is notably more intense and sharper than the (200) peak, pointing to an extended crystalline domain along the *c* axis, which is typical for anatase nanoparticles with a preferred growth in this direction.[28] On the other hand, titania powders synthesized in the presence of tris ($(HOCH_2)_3CCH_3$), trizma ($(HOCH_2)_3CNH_2$), glycine hydroxamate ($H_2NCH_2CONHOH$), and ethanolamine ($H_2N(CH_2)_2OH$) exhibit approximately equal intensities for the (004) and (200) reflections, proving that anisotropic growth along the *c* axis is slightly suppressed leading to a less elongated particle shape. This effect is most pronounced in the sample functionalized with dopamine ($(OH)_2C_6H_3(CH_2)_2NH_3Cl$), for which the (004) reflection is considerably less intense than the (200) peak, which is typical for nearly spherical particles.[28]

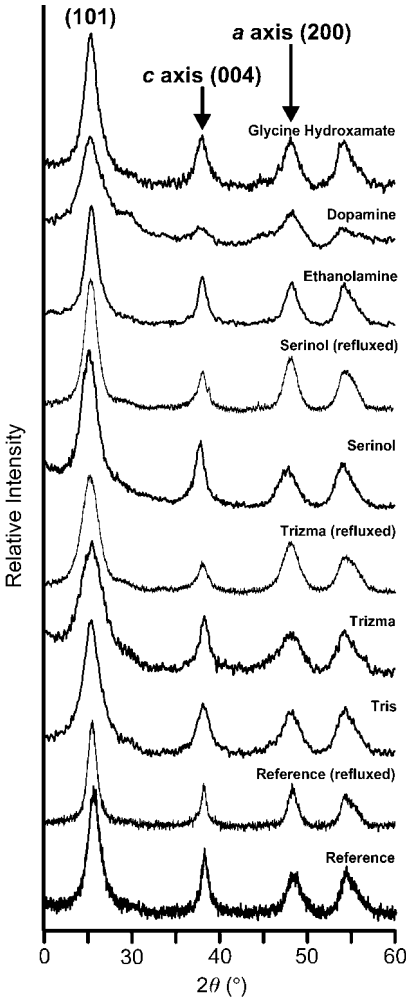

Figure 1. Powder XRD patterns of the anatase TiO_2 nanoparticles functionalized with various "assembler" ligand molecules. A Ti-to-"assembler" molar ratio of 12 was used before and after reflux.

To prove that the anisotropic growth can be quantified by XRD, diffraction patterns calculated from the Debye scattering equation are presented in Figure 2.[16,46] Although the calculations are based on model particles without accounting for a possible polydispersity of size and shape, such calculations have proven to be a useful tool in determining the preferential growth along one crystallographic direction.[16] The solid line in Figure 2 represents the calculated pattern of a spherical nanoparticle with a diameter of 3 nm. In this case, the (004) diffraction peak centered at 38° is slightly less intense than the (200) peak at 48°. In the calculated pattern of an anisotropic particle ($1.9 \times 1.9 \times 4.8$ nm) elongated along the [001] direction (dotted line in Figure 2), the relative intensities of the (004) and (200) reflections are opposite to the above, that is, the (004) diffraction peak is sharper and more intense than the (200) peak.

It is important to note that the XRD patterns of all samples, with the exceptions of the reference, trizma-, and serinol-functionalized titania particles, are similar before and after the reflux experiment (data not shown). In the cases of

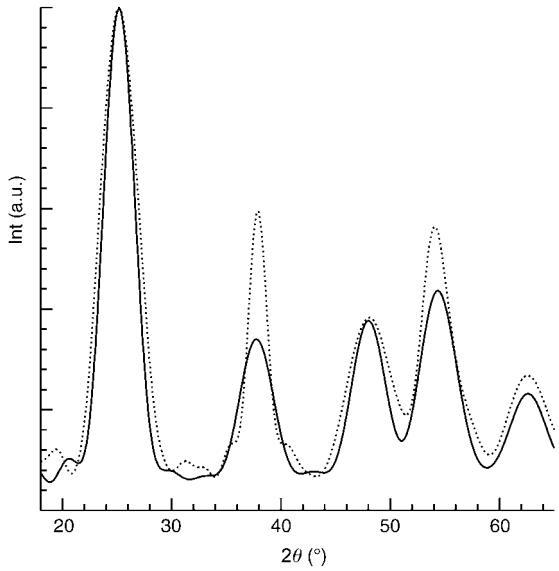

Figure 2. Diffraction patterns calculated from the Debye scattering equation for spherical nanoparticles with a diameter of 3 nm (solid line) and elongated particles (1.9×1.9×4.8 nm) along the [001] direction (dotted line).

the trizma and serinol samples, the intensity of the (004) reflection is considerably decreased after reflux, relative to the (200) reflection (Figure 1, trizma (refluxed), serinol (refluxed)). This is rather surprising, because one would expect that the fusion of the nanoparticles in the [001] direction, as observed by using high-resolution TEM (HRTEM, see below), should lead to an increase in intensity of the (004) reflection. This observation of decreased intensity points to the fact that the assembly of the nanoparticles during reflux incorporates many lattice defects, particularly in the stacking direction along the *c* axis. These defects result in a broadening of the (00l) reflections, and higher order reflections, such as the (004) peak, are particularly affected. In the case of the refluxed reference experiment, this effect is less pronounced, as the elongated primary particles aggregate in various directions (see HRTEM results below).

HRTEM was performed to evaluate the stability, shape, size, and degree of agglomeration of the nanoparticles depending on the type of ligand. The TEM image for the reference experiment without any additional "assembler" (Figure 3a) shows that the as-synthesized anatase nanocrystallites exhibit a slightly elongated shape, which is further confirmed by HRTEM measurements (Figure 3b). The particles are oriented along the [100] direction, that is, the *a* axis is perpendicular to the copper grid. Figures 3a and b reveal that the growth of the nanocrystals occurs along the *c* axis of the anatase lattice. This observation is in agreement with the experimental and calculated powder X-ray diffraction patterns. According to the presence of single spots in the power spectrum (square of the Fourier transform of the HRTEM image, Figure 3c), the lattice fringes exhibit no visible defects. The anisotropic crystal growth is governed by benzyl alcohol (BA). BA acts like a shape controller and favors the growth kinetics of TiO_2 nanoparticles in one direction (along the *c* axis) by preferential adsorption onto the {101} faces. Refluxing in water only leads apparently to uncontrolled aggregation of nanoparticles (Figure 3d), presumably due to unspecific desorption of the BA molecules from the surfaces of the nanoparticles. However, it was found that oriented attachment along the [010] and [001] directions generates porous superstructures, which are sometimes perfectly aligned with respect to the vectorial organization of the single-crystal coordinate system (Figure 3e). The presence of single spots in the power spectrum (Figure 3f) of such a porous assembly gives further evidence of a single crystal, that is, the vectorial alignment is perfect.

Based on this observation, the influence of tris and trizma on the agglomeration behavior of the anatase nanosized building blocks was examined. Tris and trizma differ only in the presence of a methyl or an amine function (see insets of Figures 4a and d, respectively). Tris is commonly used in the synthesis of tridentate metal alkoxide complexes,[47,48] and trizma is used as a buffer for cell and tissue culture,[49] but

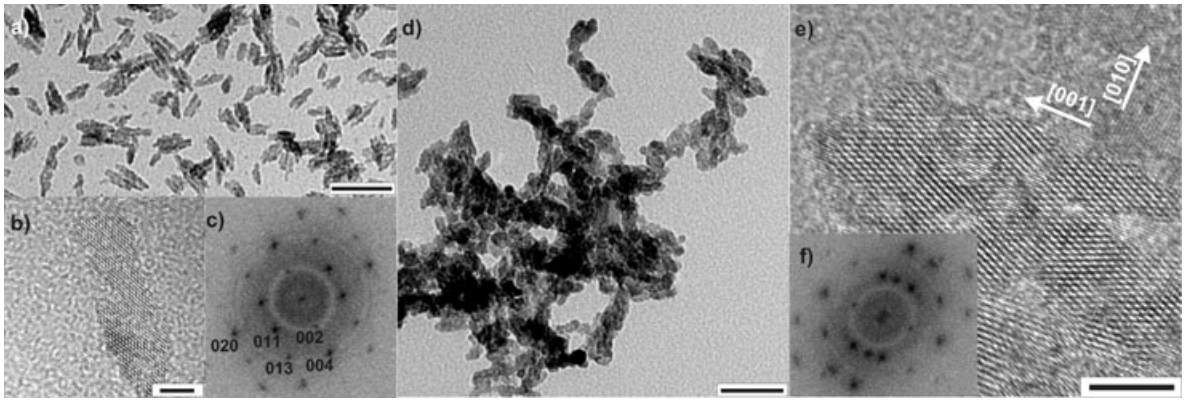

Figure 3. a) TEM image of the reference experiment (without any additional "assembler") before reflux (scale bar = 50 nm); b) HRTEM of slightly elongated nanocrystallites (scale bar = 5 nm) and c) its corresponding power spectrum; d) TEM image of the reference experiment after reflux (scale bar = 50 nm); e) HRTEM image of the reference experiment after reflux (scale bar = 5 nm) and f) its corresponding power spectrum.

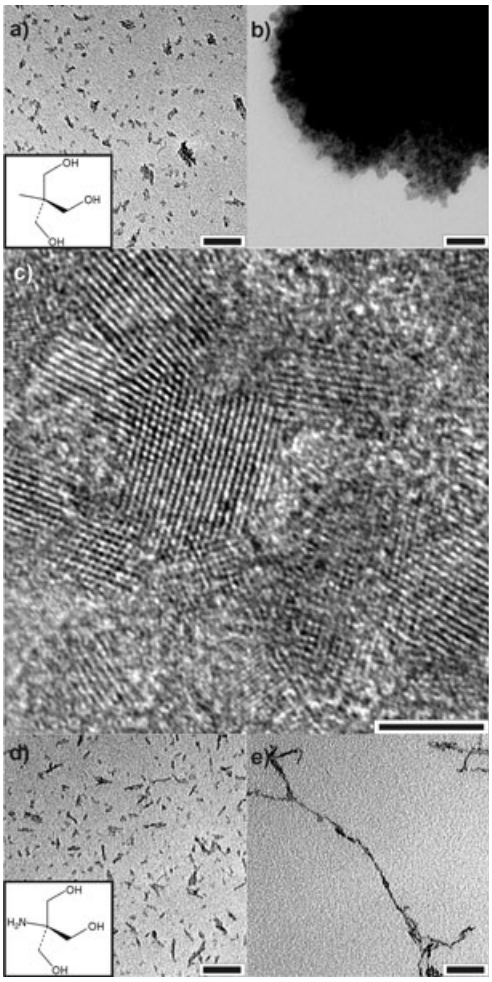

Figure 4. TEM and HRTEM images of functionalized titania nanoparticle assemblies: tris experiment a) before, and b) and c) after reflux; trizma experiment d) before and e) after reflux. The insets show schematics of the corresponding functionalizing molecules. All scale bars correspond to 50 nm, except c), in which the scale bar is 5 nm.

enhanced during the reflux procedure in water. The particles assemble into highly anisotropic nanostructures, composed of a continuous string of precisely ordered nanoparticles (Figure 4e). Considering an average particle size of about 3 nm, hundreds of nanoparticles are involved in the formation of these well-defined structures.[34] The diameter (about 3–6 nm) of the whole chain is quite uniform throughout, indicating that the nanostructure is best described as one single chain of coalesced primary particles. Some of the chains contain forks that result in the formation of branched and more complex architectures. This infrequent occurrence of branching events underlines that, in a few cases, crystal faces other than {001} can also participate in vectorial aggregation.

The presence of the free terminal amine function on the trizma-functionalized nanoparticles determines the solubility properties of the powder. Figure 5 shows trizma-functionalized titania nanoparticles dispersed in water and chloroform (Figures 5a and b, respectively) without reflux. In the case

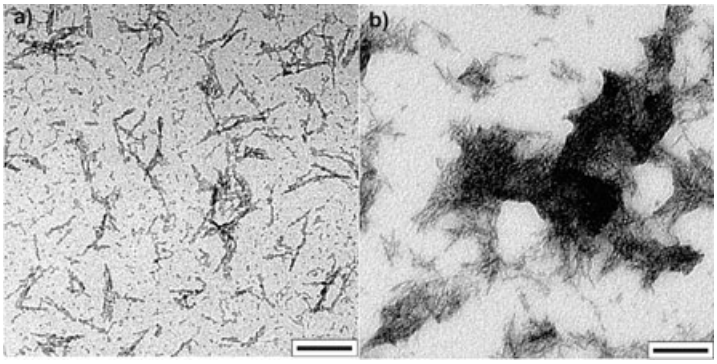

Figure 5. TEM images of as-synthesized trizma-functionalized titania nanoparticles a) dispersed in water and b) dispersed in chloroform. Scale bars = 50 nm.

they are rarely used for the functionalization of nanoparticles. The tris ligand probably plays an important role in the formation of iron oxide microplatelets consisting of perfectly aligned hematite nanoparticles.[50]

In the presence of tris, the as-synthesized nanoparticles are smaller, with an approximate size of 2.8 nm, and less agglomerated relative to the reference experiment (Figure 4a). Because tris, as a polydentate ligand, binds more strongly to titania than benzyl alcohol, the anisotropic growth is almost completely inhibited, yielding nearly spherical nanoparticles. However, upon refluxing, the tris-functionalized nanoparticles form irregularly shaped agglomerates (Figure 4b) composed of randomly oriented nanocrystals (Figure 4c).

The nanoparticles obtained in the presence of trizma exhibit similar crystallite size and shape to those obtained by tris-functionalization, but the as-synthesized particles already show anisotropic agglomeration behavior resulting in the formation of short nanorods (Figure 4d). This effect is of water, the particles immediately start to agglomerate in an anisotropic fashion forming pearl-necklace structures. The particles are just loosely connected with each other; however, initial branching events are already occurring. After one day of reflux, the nanostructures are longer, better defined, and the surface is smoother due to a better orientation of the primary particles in the pseudo-monocrystals. In chloroform, the titania nanoparticles form large, unspecific agglomerates. The amine functions on the surface of the particles evidently stabilize the particles in water but not in chloroform. The fast formation of rodlike structures in water, even at room temperature, further highlights the important role of the interplay between water and the "assembler".

To test if the presence of three hydroxymethyl groups, that is, a tripodal ligand, is a crucial prerequisite for an effective "assembler", we also investigated the influence of serinol and ethanolamine on the aggregation process. These two candidates only differ in their number of hydroxymethyl

arms, two in the serinol molecule and one in the ethanolamine molecule (see inset of Figures 6a and d, respectively). The as-synthesized nanoparticles obtained in the presence of serinol are short isolated rods composed of smaller primary particles with an average crystallite size of 3 nm (Figure 6a). The anisotropic shape of the nanocrystals is in agreement with the experimental and calculated powder X-ray diffraction patterns. After reflux, the serinol-functionalized nanoparticles assemble into isolated anisotropic nanostructures (Figure 6b), in addition to larger, apparently less-defined, aggregates. As in the case of trizma, these nanostructures exhibit monocrystal-like lattice fringes (Figure 6c), and they are formed by oriented attachment of the functionalized primary nanocrystals along the [001] direction. The ethanolamine-functionalized nanoparticles behave differently. Undefined agglomerates are found in the as-synthesized product (Figure 6d) as well as in the refluxed specimens (Figure 6e).

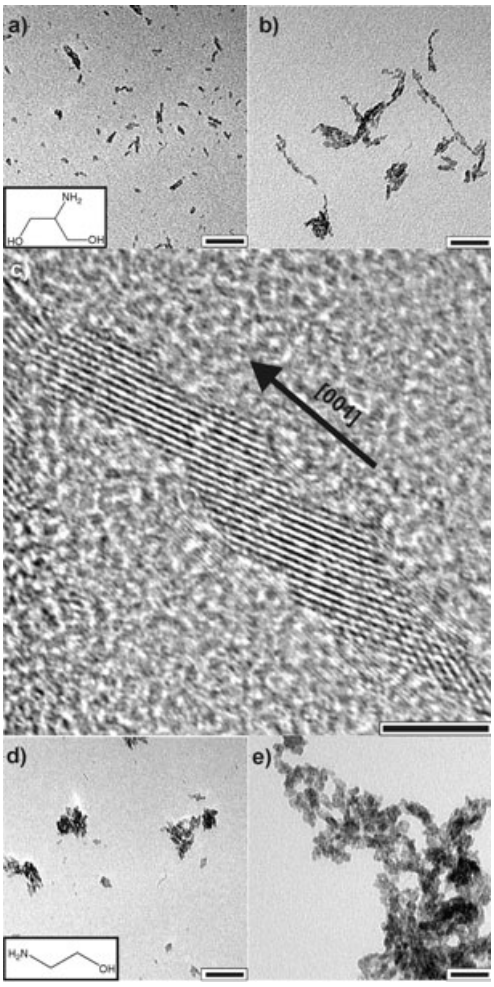

Figure 6. TEM and HRTEM images of functionalized-titania nanoparticle assemblies: serinol experiment a) before, and b) and c) after reflux; ethanolamine experiment d) before and e) after reflux. The insets show schematics of the corresponding functionalizing molecules. All scale bars correspond to 50 nm, except c), in which the scale bar is 5 nm.

Although serinol, as in the case of trizma, exhibits the ability to induce the anisotropic organization of preformed titania nanoparticles, the obtained nanostructures are less defined, generally shorter, and frequently mixed with larger, undefined agglomerates. Ethanolamine, with one $-OH$ and one $-NH_2$ group, is not able to act as an "assembler", probably due to the fact that both chemical functions can bind to the titania surface. Consequently, at least two alcohol and one amine functions are necessary to provide stability in hot water and to induce oriented attachment.

To gain further information about the adsorption of the trizma to the particle surface, X-ray photoelectron spectroscopy (XPS) and Raman measurements were performed. XPS is usually employed for the analysis of thin film and bulk materials and has rarely been applied to the surface characterization of nanoparticles. Nevertheless, it is a powerful method and generated some surprising results in this case. Figures 7 (left-to-right) depicts the N 1s, C 1s, and O 1s regions of the XP spectra of as-synthesized trizma-functionalized titania nanoparticles in comparison to nanoparticles that were obtained using benzyl alcohol only. The atomic ratios of the detected elements are summarized in Table 1.

The N 1s spectrum (Figure 7, left) of trizma-functionalized titania clearly proves that trizma is adsorbed on the surface of the titania nanoparticles. It is split into two components. The peak at 399.4 eV can be assigned to the amine function ($-NH_2$), whereas that at 401.4 eV is characteristic of the ammonium group ($-NH_3^+$).[51] The corresponding peak areas yield a NH_3^+-to-NH_2 ratio of 1.6 after exposure to the X-ray beam for 120 min. These results indicate that in addition to the protonated amine function, which stabilizes the nanoparticles in protic solvents, a significant amount of amine (~40%) is also present at the nanoparticle surface.

The C 1s (Figure 7, middle) and O 1s (Figure 7, right) XP spectra confirm the presence of trizma on the surface, in addition to benzyl alcohol. The C 1s spectrum of trizma-functionalized titania (Figure 7, middle, trizma) can be described using three peak functions centered at 284.2, 284.6, and 286.1 eV. They can be assigned to aromatic carbon, aliphatic carbon, and oxygen-bound carbon (C–OH), respectively.[52,53] In contrast, the spectrum of titania obtained in benzyl alcohol without any additional "assembler" (Figure 7, middle, BA) shows two main peaks at 284.2 and 286.1 eV (aromatic carbon and C–OH, respectively), but only a small contribution of aliphatic carbon (284.6 eV). The area of the peak associated with oxygen-bound carbon (286.1 eV) increases when trizma is added. Quantitatively, based on the peak areas, an increase in oxygen-bound carbon by a factor of 4.4 is observed. Considering the proportions of benzyl alcohol (obtained from the C-to-C–OH ratio in the reference sample) and $C-NH_2$ bond (which has a similar binding energy), a trizma-to-BA ratio of 0.75 on the nanoparticle surface is calculated. The aliphatic carbon signal is assigned to contributions from trizma and hydrocarbon impurities due to air exposure.

The O 1s spectra can be described by three peak functions centered at 530, 531.3, and 532.9 eV (Figure 7, right). They

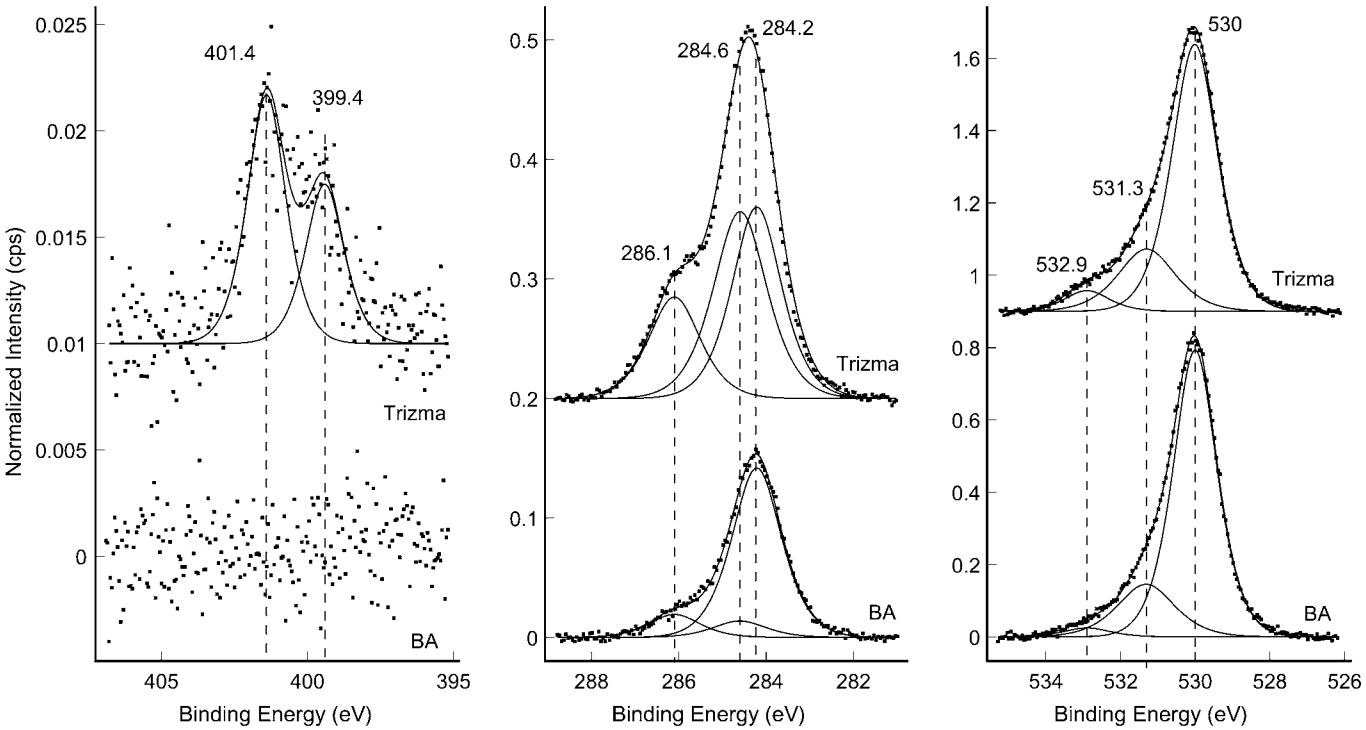

Figure 7. N 1s (left), C 1s (middle), and O 1s (right) spectra of trizma-functionalized titania (trizma) and reference experiment (BA), together with the results from the peak-fitting procedure (solid lines). The spectra of the trizma sample are offset for clarity.

Table 1. Atomic ratios [%] of the detected elements as obtained from the XPS analyses of trizma-functionalized titania (trizma) and the reference experiment (BA).

	C 1s	N 1s	O 1s	Na 1s	Cl 2p	Ti 2p
trizma	39.08	1.12	39.07	1.89	3.23	15.61
BA	22.58	0.00	50.66	2.44	3.11	21.20

can be assigned to bulk oxygen in TiO_2, oxygen in surface hydroxy groups, and oxygen in adsorbed water, respectively.[54] In the presence of trizma, an increase in the peak intensities of oxygen in hydroxyl groups (20%) and in water (120%) is observed. These results confirm the bonding of trizma to the surface. The adsorbed trizma renders the surface of the titania nanoparticles more hydrophilic, leading also to an increase in the amount of water on the nanoparticle surface. Furthermore, this enhanced hydrophilicity results in good stabilization of the nanoparticles in protic solvents.

These XPS results were confirmed by Raman spectroscopy (data not shown). Trizma-functionalized titania, as well as titania nanoparticles synthesized without any additional ligands, exhibit strong Raman bands at 1003, 1211, 1586, 1608, and 3064 cm^{-1}, due to the benzyl group.[52] In the presence of adsorbed trizma, an additional band appears at 1118 cm^{-1}, which can be assigned to aliphatic C–C stretching.[52]

To learn more about the molecular parameters that control the assembly process, other bidentate ligands with terminal amino groups, such as dopamine and glycine hydroxamate, were investigated. It has been reported that enediol ligands bind to transition-metal oxides by covalent linkages of one metal atom per enediol function, providing a simple means of modifying the surface and physical properties of the nanoparticles with specific terminal functional groups.[43,55,56] The use of dopamine and glycine hydroxamate potentially enables functionalization of the titania nanoparticles with ligands characterized by an amine function as the stabilizing terminal group and a strong anchoring part responsible for binding to the particle surface. The TEM image of the as-synthesized sample shows well-dispersed and spherical nanoparticles (Figure 8a) with an average crystallite size of 2.5 nm. The isotropic growth of the crystals is also confirmed by the experimental and calculated powder X-ray diffraction patterns. In the case of glycine hydroxamate, the TEM image reveals similarly well-dispersed nanoparticles (Figure 8d) with an average crystallite size of 3 nm. Both surface modifiers provide considerable stabilization of the nanoparticles in water by electrostatic repulsion of the amino groups.

After refluxing, the red solution of the dopamine-functionalized particles turned brown and cloudy. The TEM image (Figure 8b) reveals the presence of small, isolated particles in addition to larger, undefined agglomerates consisting of randomly attached nanocrystals (Figure 8c). On the other hand, glycine hydroxamate functionalized nanoparticles form larger, but better stabilized assemblies (Figure 8e). In spite of the strong binding of the chelates to the

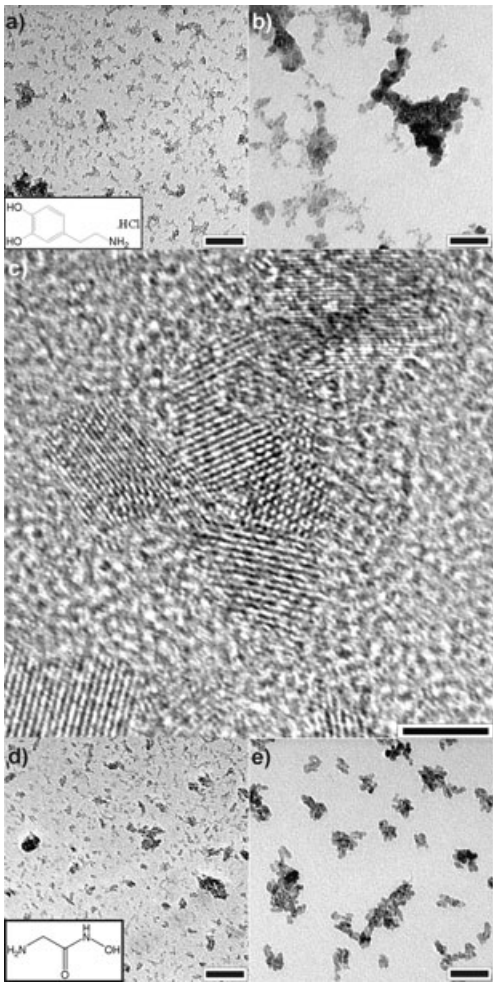

Figure 8. TEM and HRTEM images of functionalized-titania nanoparticle assemblies: dopamine experiment a) before, and b) and c) after reflux; glycine hydroxamate experiment d) before and e) after reflux. The insets show schematics of the corresponding functionalizing molecules. All scale bars correspond to 50 nm except c), in which the scale bar is 5 nm.

particle surface, combined with the presence of the terminal amino function, the reflux experiment does not result in the formation of well-defined nanostructures, unlike the case of trizma. This is probably due to the fact that in these cases the particle surfaces are less covered (see below) and less protected, as compared to trizma, and, thus, destabilization is mainly induced by desorption of the large amount of BA molecules from the particle surface.

For the surface-coverage calculation, we have to make some assumptions regarding the binding mode of the different ligands to the titania nanoparticles. Usually, chelating ligands bind to the titania surface by the so-called bridge bonding mode, that is, each OH group is coordinated to one titanium atom.[56,57] Investigations of the binding modes of polypodal alcohols on metal oxide surfaces are scarce and in the case of titania mainly restricted to the rutile phase.[58] However, it is reasonable to assume that trizma can coordinate three titanium atoms, by either three OH groups or one NH_2 and two OH groups. The two OH functions of serinol are expected to coordinate two titanium centers, whereas dopamine and glycine hydroxamate bind only to one titanium atom. Rajh et al.[55] reported that the molar concentration of the titania surface sites ($[Ti_{surf}]$) can be calculated as follows: $[Ti_{surf}] = [TiO_2] \times 12.5/d$, with $[TiO_2]$ being the molar concentration of titania and d being the diameter of the particles in angstroms. With an applied Ti-to-ligand ratio of only 12, and assuming that all $TiCl_4$ molecules are transformed into TiO_2 molecules, and all ligand molecules are linked by the proposed binding modes to titania nanoparticles (taking a mean particle diameter of 30 Å), the coverage of the particles is approximately 20% for dopamine and glycine hydroxamate, 40% for serinol, and 60% for trizma.

The ligand functionality of trizma and serinol represents a useful tool to cover and protect the particle surfaces very efficiently, whereas dopamine and glycine hydroxamate provide the lowest surface coverage. In the last two cases, there is a large amount of BA adsorbed on the particles, leading to uncontrolled agglomeration upon refluxing. Even though the relationship between surface coverage and agglomeration behavior in water is based on simple assumptions, the results obtained give a good explanation for the difference in agglomeration behavior of the various ligands in terms of ligand functionality.

In addition to the solubility and stability properties in hot water, anisotropic reactivity of the nanosized building blocks is evidently required for the formation of pseudo-1D nanostructures. In this context, two possibilities have to be considered, involving either selective binding of the "assembler" molecules to specific crystal faces or selective desorption of "assembler" molecules from specific crystal faces. It is reasonable to believe that the formation of anisotropic assemblies is not based on the selective binding of "assemblers". The basis for this assumption is that all the applied "assemblers" (except serinol) lead to the formation of more spherical particles with respect to the reference experiment. Without "assemblers", the as-synthesized particles are elongated along the [001] axis of the anatase lattice. In the presence of "assembler" molecules, the particles are nearly spherical, giving evidence that the "assembler" molecules bind nonspecifically to all crystal faces, and, thus, inhibit the anisotropic crystal growth. Consequently, the anisotropic assembly has to be induced by the selective removal of the protective shell of organic stabilizers from specific crystal faces to enhance the nanoparticles' reactivity towards oriented coalescence. Assuming that the "assemblers" stabilize all crystal faces of the building blocks, the {001} face must have some specific chemical features to allow selective desorption. For this reason, a detailed examination of the crystal structure and the relative surface energies of the crystal faces is necessary. Anatase has a tetragonal structure (the c axis being 2.7 times the a axis) and has been shown to nucleate as truncated bipyramidal seeds,[33] exposing eight equivalent {101} and two equivalent {001} faces. According to Donnay and Harker rules,[59] the surface free energy of the {001} faces is ~1.4 times larger than that of the {101} faces.

This lower stability is an important feature on the pathway to the oriented attachment of titania nanosized building blocks in a crystallographically controlled manner. Based on the geometrical construction shown in Figure 9b, it is possible to provide a simple scheme to visualize the morphology of the primary particles (Figure 9a) as well as the assembly process (Figures 9c and d).

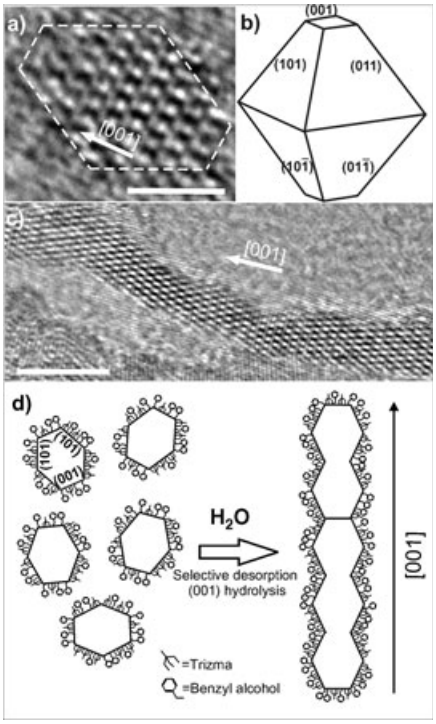

Figure 9. a) HRTEM image of a trizma-functionalized titania nanoparticle (scale bar = 2 nm). b) The equilibrium shape of a TiO_2 crystal in the anatase phase according to the Wulff construction. c) HRTEM image of a trizma-functionalized titania nanoparticle assembly (scale bar = 5 nm). d) Proposed formation mechanism from the building blocks to the anisotropic nanostructure.

The important role of water in the formation of anisotropic nanostructures has been highlighted here. Water seems to play two roles, namely, separation of the building blocks in a polar medium and replacement of the stabilizers on the {001} faces, enhancing the anisotropy of aggregation. Theoretical calculations indicated a significant difference in the adsorption of water on the {101} and {001} faces. Water adsorbs molecularly on the (101) surface and dissociates on the (001) surface.[60] H_2O dissociative adsorption induces the presence of hydroxyl groups on the (001) plane, which provide a potential reactive site for particle attachment. It is reasonable to assume that anisotropic organization of the nanoparticles is initiated by a decrease in the amount of stabilizers on the (001) plane and by the activation of the OH groups on this plane. The aggregation/fusion process is then given by, first, a removal of high-surface-energy planes and, second, by the removal of solvents and the formation of chemical bonds by OH-condensation at the interface between primary particles.[32]

Conclusion

In this work we present detailed investigations on the assembly properties of preformed TiO_2 nanopowders in terms of their dependence on ligand functionality. A systematic variation of the organic "assembler" molecules bound to the surface of the anatase nanocrystals shows that four parameters play a particularly important role: 1) the type and number of "assembler" functional groups, 2) the surface coverage of the nanoparticles by the "assembler", 3) the surface energy of the anatase crystal faces, and 4) the surface reactivity of the different crystal faces towards water.

As the examples of trizma and serinol show, surface functionalization by means of polyalcohols with terminal amino groups results in the formation of anisotropic nanostructures. As tris-functionalized nanoparticles do not assemble anisotropically, the additional functionality provided by the amino group is clearly the key to providing sufficient stabilization for a controlled process. However, the presence of an amino group alone is not enough to induce anisotropic particle arrangement, the other prerequisite is good surface coverage of the nanoparticulate building blocks. Therefore, dopamine and glycine hydroxamate, with their low coverage of particle surface, are not able to induce nanowire formation in spite of their amino groups. These organic species even prevent any kind of oriented attachment and just allow the formation of random assemblies upon reflux. This observation is in agreement with previous reports, in which organic additives such as glycine, acetic acid, and adipic acid suppressed the hydrothermal coarsening of titania nanocrystals by oriented attachment.[33] On the other hand, it is notable that oriented attachment also occurs in the reference sample without any "assembler" during reflux. In this case, however, particles fuse in all directions generating porous crystalline superstructures. In addition to the role of the "assemblers", the peculiar features of the anatase crystal structure are also relevant. It is, ultimately, the increased reactivity of the titania {001} faces that allows trizma and serinol to act successfully as assembling agents.

Another important aspect of this work is the evaluation and comparison of X-ray diffraction and HRTEM results. It is found that, although in HRTEM the particles are identified as perfectly vectorially aligned, XRD peaks of higher order crystal planes perpendicular to the fiber direction are weakened and less defined. This is attributed to lattice defects that are presumably typical for the special mode of nanofiber growth by particle alignment. It has to be checked with other systems undergoing controlled alignment whether this criterion can be used to identify this special mode of crystallization.

In addition, we are able to show that XPS can be employed to gain information about the different organic species attached to the surface of the nanoparticles, their rela-

tive ratio, and even about the functional groups that are involved in the binding. Therefore, it will be possible to explain the different efficiencies of various potential "assembler" molecules with sometimes very similar chemical structures.

To conclude, the synthesis of powders consisting of nanoparticles, which have their assembly behavior already encoded by functional molecules on their surfaces, would be an immense step forward toward the controlled, bottom-up fabrication of well-defined nanostructures. In this work we highlighted some novel, but crucial, aspects and principal physicochemical phenomena occurring on the long way to self-organization of individual nanoparticle components into nanodevices.

Experimental Section

Materials: Titanium(IV) chloride ($TiCl_4$, 99.9%), anhydrous benzyl alcohol (BA, 99.8%), 1,1,1-tris(hydroxymethyl)ethane (tris, 99%), 2-amino-2-(hydroxymethyl)-1,3-propanediol (trizma, 99.9%), 3-hydroxytyramine hydrochloride (dopamine, 98%), glycine hydroxamate (>90%), 2-amino-1,3-propanediol (serinol, 98%), ethanolamine (99.5%), and the solvents (analytical grade) were purchased from Sigma-Aldrich. All chemicals were used without further purification.

Synthesis of functionalized TiO_2 nanocrystals: In a typical synthesis, the ligand (0.38 mmol, i.e., Ti-to-ligand molar ratio of 12) was dispersed in benzyl alcohol (10 mL). The ligands used were tris, trizma, dopamine, glycine hydroxamate, serinol, and ethanolamine. In the next step, $TiCl_4$ (0.5 mL, 4.55 mmol) was slowly added to the benzyl alcohol and ligand mixture under vigorous stirring at room temperature. The vial was sealed and the mixture was heated to 80°C under continuous stirring. The aging time was 24 h. The resulting suspension was centrifuged and the precipitate was thoroughly washed twice with chloroform. After each washing step, the solvent was removed by centrifugation. The collected material was left to dry in air at 60°C and finally ground into a fine powder.

Synthesis of anisotropic TiO_2 nanostructures: For the assembly process, the functionalized titania nanoparticles (65 mg) were dispersed in distilled water (12.5 mL) and refluxed for 24 h under stirring.

Characterization: The powder X-ray diffraction diagrams of all samples were measured in reflection mode ($Cu_{K\alpha}$ radiation) on a Bruker D8 diffractometer equipped with a scintillation counter. XRD patterns were obtained in the 2θ range of 20–60° by step scanning with a step size of 0.01°. Transmission electron microscopy investigations were performed either on an Omega 912 (Carl Zeiss) microscope, operated at 100 kV (TEM), or on a Philips CM200 FEG microscope, operated at 200 kV (HRTEM). For the functionalized TiO_2 nanocrystals, the fine powders were dispersed in ethanol and one drop of this dispersion was deposited on a TEM grid. Refluxed TiO_2 dispersions were further diluted with water and one drop was deposited on a TEM grid, supported by filter paper for fast drying. X-ray photoelectron spectroscopy measurements were carried out by using a modified LHS/SPECS EA200 MCD system equipped with a $Mg_{K\alpha}$ source (1253.6 eV, 168 W). The pass energy of the analyzer was fixed to 48 eV. The binding energy scale of the system was calibrated with foil samples of Au ($4f_{7/2}$ = 84.0 eV) and Cu ($2p_{3/2}$ = 932.67 eV). The functionalized TiO_2 powder samples were mounted on a stainless steel sample holder. The base pressure of the UHV chamber was 1×10^{-10} mbar. All binding energies were referenced to the O 1s peak of the oxygen component of anatase TiO_2 at 530.0 eV.[54] The shifts in binding energy due to charging effects amounted to 1.63 and 1.27 eV for trizma-functionalized titania and titania obtained by using only benzyl alcohol, respectively. The spectra were normalized to yield the same Ti intensity. Quantitative data analysis was performed by subtracting a stepped background and using empirical cross sections.[61] For Raman spectroscopy, the spectrometer (LabRam, Jobin Yvon) was equipped with a HeNe laser (632.8 nm). The laser was operated at a power level of 10 mW measured at the position of the sample. The spectral resolution of the spectrometer was 1 cm^{-1}. Sampling times varied between 500–1000 s.

Acknowledgements

Financial support by the Max-Planck-Society and by the DFG (Schwerpunktprogramm SPP 1165 "Nanodrähte und Nanoröhren") is gratefully acknowledged. We thank Drs. Bernd Smarsly and Helmut Cölfen for helpful discussions. We are indebted to Ms. Dörte Beilfuss for the design of the graphic displayed on the cover page.

[1] H. Weller, *Angew. Chem.* **1996**, *108*, 1159–1161; *Angew. Chem. Int. Ed. Engl.* **1996**, *35*, 1079–1081.
[2] S. A. Davis, M. Breulmann, K. H. Rhodes, B. Zhang, S. Mann, *Chem. Mater.* **2001**, *13*, 3218–3226.
[3] C. Sanchez, G. Soler-Illia, F. Ribot, T. Lalot, C. R. Mayer, V. Cabuil, *Chem. Mater.* **2001**, *13*, 3061–3083.
[4] G. M. Whitesides, B. Grzybowski, *Science* **2002**, *295*, 2418–2421.
[5] B. A. Parviz, D. Ryan, G. M. Whitesides, *IEEE Trans. Adv. Packag.* **2003**, *26*, 233–241.
[6] G. R. Patzke, F. Krumeich, R. Nesper, *Angew. Chem.* **2002**, *114*, 2554–2571; *Angew. Chem. Int. Ed.* **2002**, *41*, 2446–2461.
[7] C. N. R. Rao, F. L. Deepak, G. Gundiah, A. Govindaraj, *Prog. Solid State Chem.* **2003**, *31*, 5–147.
[8] Y. N. Xia, P. D. Yang, Y. G. Sun, Y. Y. Wu, B. Mayers, B. Gates, Y. D. Yin, F. Kim, Y. Q. Yan, *Adv. Mater.* **2003**, *15*, 353–389.
[9] C. N. R. Rao, M. Nath, *Dalton Trans.* **2003**, 1–24.
[10] Z. L. Wang, *Adv. Mater.* **2003**, *15*, 432–436.
[11] Y. Y. Wu, H. Q. Yan, M. Huang, B. Messer, J. H. Song, P. D. Yang, *Chem. Eur. J.* **2002**, *8*, 1261–1268.
[12] Z. R. Dai, Z. W. Pan, Z. L. Wang, *Adv. Funct. Mater.* **2003**, *13*, 9–24.
[13] F. Krumeich, H. J. Muhr, M. Niederberger, F. Bieri, B. Schnyder, R. Nesper, *J. Am. Chem. Soc.* **1999**, *121*, 8324–8331.
[14] L. Manna, E. C. Scher, A. P. Alivisatos, *J. Am. Chem. Soc.* **2000**, *122*, 12700–12706.
[15] S.-J. Park, S. Kim, S. Lee, Z. G. Khim, K. Char, T. Hyeon, *J. Am. Chem. Soc.* **2000**, *122*, 8581–8582.
[16] N. Pinna, U. Wild, J. Urban, R. Schlögl, *Adv. Mater.* **2003**, *15*, 329–331.
[17] Z. Y. Tang, N. A. Kotov, M. Giersig, *Science* **2002**, *297*, 237–240.
[18] Z. Y. Tang, B. Ozturk, Y. Wang, N. A. Kotov, *J. Phys. Chem. B* **2004**, *108*, 6927–6931.
[19] C. Pacholski, A. Kornowski, H. Weller, *Angew. Chem.* **2002**, *114*, 1234–1237; *Angew. Chem. Int. Ed.* **2002**, *41*, 1188–1191.
[20] A. Taden, K. Landfester, M. Antonietti, *Langmuir* **2004**, *20*, 957–961.
[21] S. Wohlrab, N. Pinna, M. Antonietti, H. Cölfen, *Chem. Eur. J.*, in press, DOI: 10.1002/chem.200400420.
[22] Z. B. Zhang, C. C. Wang, R. Zakaria, J. Y. Ying, *J. Phys. Chem. B* **1998**, *102*, 10871–10878.
[23] A. Hagfeldt, M. Grätzel, *Acc. Chem. Res.* **2000**, *33*, 269–277.
[24] E. W. McFarland, J. Tang, *Nature* **2003**, *421*, 616–618.
[25] S. U. M. Khan, M. Al-Shahry, W. B. Ingler, Jr., *Science* **2002**, *297*, 2243–2245.
[26] M. Ferroni, M. C. Carotta, V. Guidi, G. Martinelli, F. Ronconi, M. Sacerdoti, E. Traversa, *Sens. Actuators B* **2001**, *77*, 163–166.
[27] D. G. Shchukin, J. H. Schattka, M. Antonietti, R. A. Caruso, *J. Phys. Chem. B* **2003**, *107*, 952–957.
[28] P. D. Cozzoli, A. Kornowski, H. Weller, *J. Am. Chem. Soc.* **2003**, *125*, 14539–14548.
[29] Y. W. Jun, M. F. Casula, J. H. Sim, S. Y. Kim, J. Cheon, A. P. Alivisatos, *J. Am. Chem. Soc.* **2003**, *125*, 15981–15985.
[30] R. L. Penn, J. F. Banfield, *Science* **1998**, *281*, 969–971.

[31] R. L. Penn, J. F. Banfield, *Am. Mineral.* **1998**, *83*, 1077–1082.
[32] R. L. Penn, *J. Phys. Chem. B* **2004**, *108*, 12707–12712.
[33] R. L. Penn, J. F. Banfield, *Geochim. Cosmochim. Acta* **1999**, *63*, 1549–1557.
[34] J. Polleux, N. Pinna, M. Antonietti, M. Niederberger, *Adv. Mater.* **2004**, *16*, 436–439.
[35] J. Joo, T. Yu, Y. W. Kim, H. M. Park, F. X. Wu, J. Z. Zhang, T. Hyeon, *J. Am. Chem. Soc.* **2003**, *125*, 6553–6557.
[36] J. Tang, J. Fabbri, R. D. Robinson, Y. M. Zhu, I. P. Herman, M. L. Steigerwald, L. E. Brus, *Chem. Mater.* **2004**, *16*, 1336–1342.
[37] N. Pinna, M. Antonietti, M. Niederberger, *Colloids Surf. A* **2004**, *250*, 211–213.
[38] N. Pinna, G. Garnweitner, M. Antonietti, M. Niederberger, *Adv. Mater.* **2004**, *16*, 2196–2200.
[39] M. Niederberger, N. Pinna, J. Polleux, M. Antonietti, *Angew. Chem.* **2004**, *116*, 2320–2323; *Angew. Chem. Int. Ed.* **2004**, *43*, 2270–2273.
[40] M. Niederberger, G. Garnweitner, N. Pinna, M. Antonietti, *J. Am. Chem. Soc.* **2004**, *126*, 9120–9126.
[41] M. Niederberger, M. H. Bartl, G. D. Stucky, *Chem. Mater.* **2002**, *14*, 4364–4370.
[42] M. Niederberger, M. H. Bartl, G. D. Stucky, *J. Am. Chem. Soc.* **2002**, *124*, 13642–13643.
[43] M. Niederberger, G. Garnweitner, F. Krumeich, R. Nesper, H. Cölfen, M. Antonietti, *Chem. Mater.* **2004**, *16*, 1202–1208.
[44] N. Pinna, G. Neri, M. Antonietti, M. Niederberger, *Angew. Chem.* **2004**, *116*, 4445–4449; *Angew. Chem. Int. Ed.* **2004**, *43*, 4345–4349.
[45] A. Pottier, S. Cassaignon, C. Chaneac, F. Villain, E. Tronca, J.-P. Jolivet, *J. Mater. Chem.* **2003**, *13*, 877–882.
[46] W. Vogel, *Cryst. Res. Technol.* **1998**, *33*, 1141–1154.
[47] T. J. Boyle, R. W. Schwartz, R. J. Doedens, J. W. Ziller, *Inorg. Chem.* **1995**, *34*, 1110–1120.
[48] A. Cornia, D. Gatteschi, K. Hegetschweiler, L. Hausherr Primo, V. Gramlich, *Inorg. Chem.* **1996**, *35*, 4414–4419.
[49] V. Santoni, M. Molloy, T. Rabilloud, *Electrophoresis* **2000**, *21*, 1054–1070.
[50] M. Niederberger, F. Krumeich, K. Hegetschweiler, R. Nesper, *Chem. Mater.* **2002**, *14*, 78–82.
[51] A. Vidyadhar, K. H. Rao, I. V. Chernyshova, *Colloids Surf. A* **2003**, *214*, 127–142.
[52] D. Lin-Vien, N. B. Colthup, W. G. Fateley, J. G. Graselli, *The Handbook of Infrared and Raman Characteristic Frequencies of Organic Molecules*, Academic Press, Boston, **1991**.
[53] T. L. Barr, *Modern ESCA*, CRC, Boca Raton, **1994**.
[54] R. Sanjinés, H. Tang, H. Berger, F. Gozzo, G. Margaritondo, F. Lévy, *J. Appl. Phys.* **1994**, *75*, 2945–2951.
[55] T. Rajh, L. X. Chen, K. Lukas, T. Liu, M. C. Thurnauer, D. M. Tiede, *J. Phys. Chem. B* **2002**, *106*, 10543–10552.
[56] M. J. McWhirter, P. J. Bremer, I. L. Lamont, A. J. McQuillan, *Langmuir* **2003**, *19*, 3575–3577.
[57] J. P. Folkers, C. B. Gorman, P. E. Laibinis, S. Buchholz, G. M. Whitesides, R. G. Nuzzo, *Langmuir* **1995**, *11*, 813–824.
[58] U. Diebold, *Surf. Sci. Rep.* **2003**, *48*, 53–229.
[59] J. D. Donnay, D. Harker, *Am. Mineral.* **1937**, *22*, 446–468.
[60] A. Vittadini, A. Selloni, F. P. Rotzinger, M. Grätzel, *Phys. Rev. Lett.* **1998**, *81*, 2954–2957.
[61] D. Briggs, M. P. Seah, *Practical Surface Analysis*, Wiley, Chichester, **1990**.

Received: October 15, 2004
Published online: February 25, 2005

